Optoacoustic imaging quality enhancement based on geometrical super-resolution method

Hailong He[a,b], Subhamoy Mandal[a,b], Andreas Buehler[a,b], X. Luís Deán-Ben[a,b], Daniel Razansky[a,b], and Vasilis Ntziachristos*[a,b]

[a]Institute for Biological and Medical Imaging, Helmholtz Zentrum München, Ingoldstädter Landstraße 1, 85764 Neuherberg, Germany
[b]Chair for Biological Imaging, Technische Universität München, Ismaninger Str. 22, 81675 München, Germany

ABSTRACT

In optoacoustic imaging, the resolution and image quality in a certain imaging position usually cannot be enhanced without changing the imaging configuration. Post-reconstruction image processing methods offer a new possibility to improve image quality and resolution. We have developed a geometrical super-resolution (GSR) method which uses information from spatially separated frames to enhance resolution and contrast in optoacoustic images. The proposed method acquires several low resolution images from the same object located at different positions inside the imaging plane. Thereafter, it applies an iterative registration algorithm to integrate the information in the acquired set of images to generate a single high resolution image. Herein, we present the method and evaluate its performance in simulation and phantom experiments, and results show that geometrical super-resolution techniques can be a promising alternative to enhance resolution in optoacoustic imaging.

Keywords: optoacoustic imaging, super resolution, image quality enhancement

1. INTRODUCTION

Optoacoustic imaging (OA; also known as Photoacoustics) is capable of resolving chromophoric agents across a wide range of depths ranging from micrometer to centimeters scales [1, 2]. This technique has been widely used in biological research to noninvasively resolve anatomical, physiological and molecular information in biological tissue. In optoacoustic imaging, tissue is typically irradiated with nanosecond laser pulses. After absorption of the light energy, broadband ultrasonic waves are generated via a thermoelastic expansion. The ultrasonic waves are then detected with ultrasound detectors and used to reconstruct the map of the light deposition [1].

Currently, all approaches to improve the image quality and resolution are concentrated on modifying the unprocessed optoacoustic waves by utilizing advanced setups and reconstruction algorithms [3-5]. However, post-reconstruction image processing methods offers the possibility of further improving the image quality and resolution. Super-resolution (SR) is one of the most successful techniques, which can integrate information from several low resolution (LR) images obtained at different imaging positions to generate a high resolution (HR) image [6-8]. This technique offers the possibility to break the resolution limit determined by the imaging setup and reconstruction algorithms. This idea was first introduced to digital image processing and has widely used in other imaging modalities now, like CT, MRI and PET [8-10]. For example, SR methods have been successfully applied to MRI for resolution and image quality enhancement without increasing the acquisition time or changing the imaging system. These post-processing methods show better performance over direct HR acquisition when SNR and acquisition times are taken into account.

In the state of the art optoacoustic imaging scanners, objects are usually imaged at different positions through shifting and rotating the detector (or the sample). The resolution and image quality in a certain imaging position usually cannot be enhanced without changing the imaging configuration. However, images acquired at different positions may contain their unique information. The SR method can integrate the unique information from different imaging positions to reconstruct a high resolution image, which results in possible improvements in resolution and image quality. In this paper, we consider the PSR implementation in optoacoustic imaging and aimed to investigate the possible improvements

Photons Plus Ultrasound: Imaging and Sensing 2016, edited by Alexander A. Oraevsky, Lihong V. Wang
Proc. of SPIE Vol. 9708, 97082A · © 2016 SPIE · CCC code: 1605-7422/16/$18 · doi: 10.1117/12.2211626

gained in image resolution and contrast. In particular we consider the exploration of complementary information contained in adjacent images in a PSR formulation. The study involved simulations and experimental measurements on phantoms and ex-vivo organs.

2. MATERIALS AND METHODS

2.1 Super resolution method

SR techniques obtain a high resolution image from low resolution image sequences acquired from different imaging views. The general SR model is an inverse process of imaging degradation, and a regularization term is usually imposed to obtain a stable solution for the ill-posed SR problem. Accordingly, the SR process can be modeled as follow [6, 8]:

$$\overline{X} = \arg\min_{X} \{ \sum_{k=1}^{N} \left\| Y_k, D_k H_k F_k X \right\| + \lambda \gamma(X) \} \tag{1}$$

Where $\{Y_k\}$ represents the kth LR image, with resolution $N_1 \times N_2$, and X is the HR image estimated from $\{Y_k\}$, with resolution $qN_1 \times qN_2$, q is the sampling scalar. D_k represents the decimation operator, H_k is the blur matrix representing the point spread function (PSF) of the imaging system. For simplicity, the H_k kernel is taken as delta function with a width of one pixel. F_k is the geometric motion operator between the estimated HR frame X and the kth LR frame. V_k is the system additive noise. $\gamma(X)$ is a regularization term in the SR process. λ is a regularization weighing parameter, which is determined according to the trade-off between edge information and noise. Even though the spatial transformation information of different imaging modes for all measurements is known, they are not accurate enough to reflect the real motion information between each reconstruction images. Therefore, motion estimation method is first applied to calculate the F_k motion matrix between the estimated HR frame X and the kth LR frame Y. The estimated HR frame X is updated by integrating the difference information between the estimated HR frame X and each LR images. This process is repeated iteratively until the minimization function in (1) reaches a predefined threshold or after a maximum number of iterations.

The SR inversion process defined in Eq. (1) is an ill-posed process, so that a regularization term is generally required for rendering a stable solution [6]. The regularization term compensates for ill-posedness by a priori imposing additional information on the desirable HR image [6, 11], consequently suppressing artifacts and noise, and improving the rate of convergence. Herein, we employ a bilateral total variation (BTV) regularization term defined as [6, 11]:

$$\gamma(X) = \sum_{l=-P}^{P} \sum_{m=0}^{P} \alpha^{|m|+|l|} \left\| X - S_x^l S_y^m X \right\| \tag{2}$$

where $l + m \geq 0$, S_x^l and S_y^m are shift matrices to present l and m pixels shift in horizontal and vertical directions, respectively. $P(1 \leq P \leq 3)$ is the shifting range in both directions and $\alpha(0 < \alpha < 1)$ is the weighting coefficient. The scalar weight α gives a spatially-decaying effect to the regularization terms summation. The BTV regularization is based on the combination of the total variation restoration model and the bilateral filter [6, 11], where total variation anisotropic diffusion is used for image restoration and edge enhancement, and the bilateral filter focuses on noise reduction and edge sharpening [6, 7]. Subsequent application of the bilateral filter several times leads to smoothing of the signal until reaching a steady rate. Based on this, a large value of α is chosen for images affected by noise, which suppresses noise and smooth flat regions in the estimated HR image at the expense of losing edge information. More detailed information about the BTV regularization function can be found elsewhere [6, 7]. Combining Eqs. (1) and (2), the iterative PSR process is calculated with steepest descent method and the final minimization function described as [6, 11]:

$$\overline{X}_{n+1} = \overline{X}_n + \left\{ \sum_{k=1}^{N} F_k^T H_k^T D_k^T \bullet sign(Y_k - D_k H_k F_k \overline{X}_n) + \lambda \left(\sum_{l=-P}^{P} \sum_{m=0}^{P} \alpha^{|m|+|l|} (I - S_x^{-l} S_y^{-m}) \bullet sign(\overline{X}_n - S_x^l S_y^m \overline{X}_n) \right) \right\} \tag{3}$$

where S_x^{-l} and S_y^{-m} represent the transposes of matrices S_x^l and S_y^m respectively and they have a shifting effect in the opposite directions as S_x^l and S_y^m.

2.2 Simulation and phantom measurement

A simulation study was conducted to test the SR theory for optoacoustic imaging. The resolution target phantom was used to define the initial optoacoustic pressure distribution shown in Fig. 1(a). The simulations were computed in MATLAB using the k-Wave Toolbox [12]. The object was simulated in 3 positions with linearly distance of 300um in the same imaging plane. At each position, signals were detected using a 180 degree curve of 200 evenly distributed point detectors with a radius of 25 mm. A simulated Gaussian impulse response of the point detector is convolved with the simulated optoacoustic signals to model the practical detector detection. Then three optoacoustic images were reconstructed with filter backprojection method with pixel width 100 μm (80×50 pixels). These three reconstructed images were used for the SR reconstruction and the one in the middle imaging position was chosen as the reference image. The final SR image is up-sampled two times of the LR image, as well as the interpolation and interleaving results.

The phantom and tissue experiments were conducted using a commercial small animal multispectral optoacoustic tomography (MSOT) scanner (Model: MSOT256-TF, iThera Medical GmbH, Munich, Germany). The scanner utilizes cross-sectional optoacoustic acquisition geometry and consists of a custom-made 256-element array of cylindrically-focused piezocomposite transducers with 5 MHz central frequency for simultaneous acquisition of the signals generated with each laser pulse. The transducer array covers an angle of approximately 270° and has a radius of curvature of 40 mm. Light excitation is provided with the output laser beam from a wavelength-tunable optical parametric oscillator - based laser, which is shaped to attain ring-type uniform illumination on the surface of the phantoms by means of a custom-made fiber bundle. The detected optoacoustic signals are simultaneously digitized at 40 Mega samples per second. The scanner is capable of rendering 10 cross-sectional images per second but here the images were averaged 10 times in order to improve SNR performance in acquiring entire mouse cross sections. More detail information about the imaging setup can be found elsewhere [3, 13, 14]

In order to test the SR method for improving image quality, a paper phantom with complex geometrical structure was imaged shown in Fig 2. The phantom was imaged by MSOT setup in different translation positions (with accurate step size 0.3 mm). As the MSOT detectors are toroidally focused, normally the best quality image can be obtained when the sample is put on the focus area of the detector. In order to show a fair comparison, the best quality cross-sectional reconstruction result was chosen as the reference image for the SR process. Another scans of the phantom were picked up before and after the position of the reference image. Signals of 200 channels in the middle area of the detector were used for reconstruction. And three optoacoustic images were reconstructed with pixel width 100 μm (100×100 pixels). Further trials on an ex-vivo murine kidney were conducted to test the practicability and efficacy of the method in realistic biological tissues. The kidney was extracted post-mortem according to institutional regulations regarding animal handling protocols and subsequently embedded in a diffuse agar block (6% by volume Intralipid in the agar solution) for ensuring uniform illumination of the sample. After completion of OA imaging experiment, the sample was isolated and frozen in -51° C for 24 hours. It was thereafter embedded in a water soluble optimal cutting temperature compound and cryosectioned with sample thickness of 20 μm at a temperature of -20° C. The RGB images of the cryosections were used as a reference to validate the reconstruction and PSR results by correlating the location, orientation and morphology of the blood vessels within the kidney mass.

All LR images were mathematically registered to the reference image for calculation of the image transformation. For comparison, the transformation information between the reference image and each LR images were interpolated into the reference image to obtain the so-called interleaving image. The interleaving image corresponds to a two times up-sampled LR image with the same size as the PSR image. λ was taken as 0.02 for all data, while α was taken as 0.01 for the simulated LR images and, was increased to 0.05 for smoothing noise of the reconstructed PSR images in the phantom experiment.

3. RESULTS

The results of the simulated phantom obtained in three linear positions of the same imaging plane are depicted in Fig. 1. The standard OA image reconstructed by using the backprojection algorithm with the processing and filtering (filtering cutoffs) as the SR image is shown in Fig. 1(b), this image is used as the reference image for SR reconstruction. The

interleaving image is shown in Fig .1(c). And the SR image reconstructed from the same 3 slices is shown in Fig. 1(d). From those images, it clearly shows that line targets in the SR result are better resolved comparing to other images. The lateral and axial profiles marked by the dash red lines in Fig. 1(d) demonstrate that significant resolution improvement is achieved in the SR result comparing to other images.

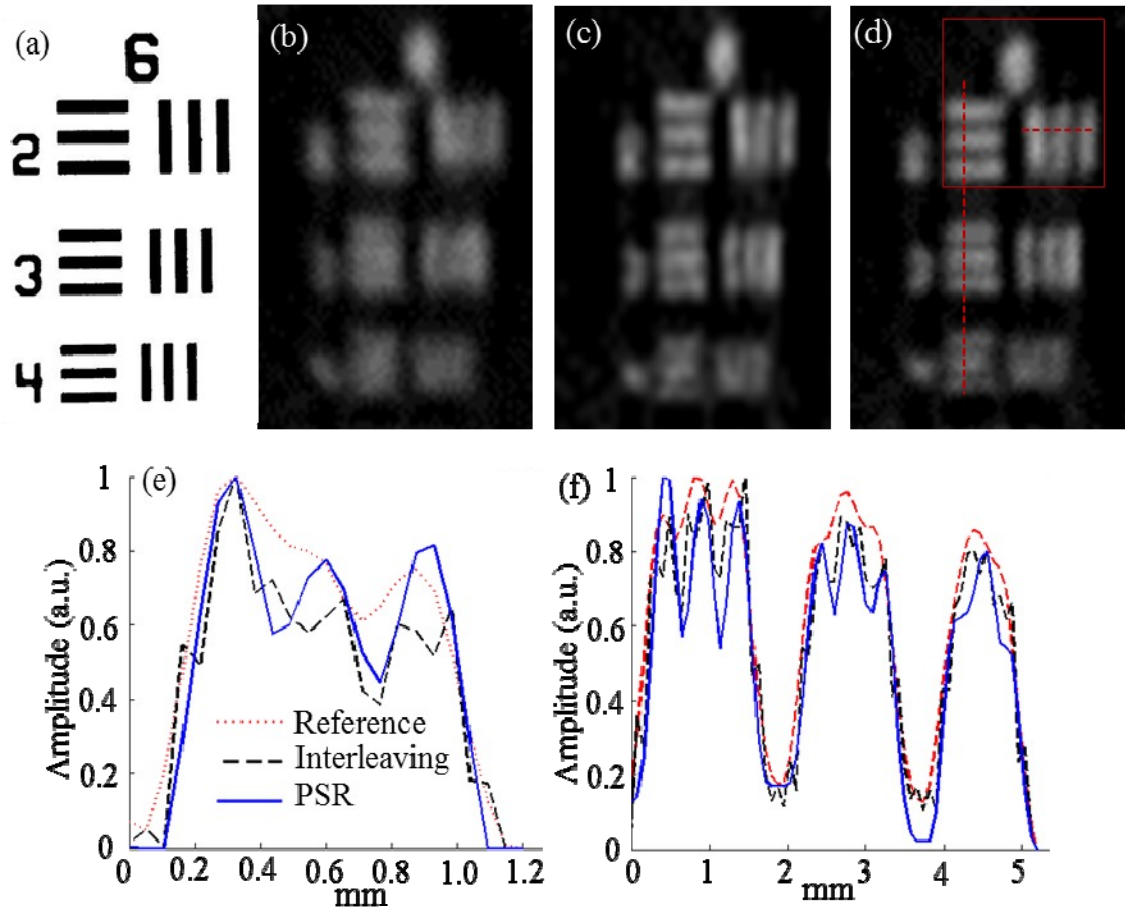

Figure 1: Simulation of Super-resolution (SR) algorithm: (a) The reference USAF phantom, (b)the reference image (pixel width 100um, 160×100 pixels), 3 LR images with 3pixels shifts were used to obtain a higher resolution image using (c) interleaving, (d) SR. The line profiles in (e) horizontal and (f) vertical directions are represented for the three different methods outlined in the study.

The paper phantom with complex structure is utilized to prove the practicability of SR methods for improving the image quality. The phantom structure and detector position are illustrated in Fig. 2(a). Due to limited view problem, the reference image shown in Fig. 2(b) is distorted comparing to the real structure, like the structure of the line object (white arrow) is not continued. Fig. 2(c) shows the interleaving result with 3 LR images. The SR result is shown in Fig. 2(d). The visibility of the SR image is significantly improved. Comparing to other results, features of the SR image are better recovered by integrating information from different imaging views. For example, the line structure is better resolved and the contrast of targets (i.e. the area enclose by the red ellipse as marked in Fig.2) shows a great improvement.

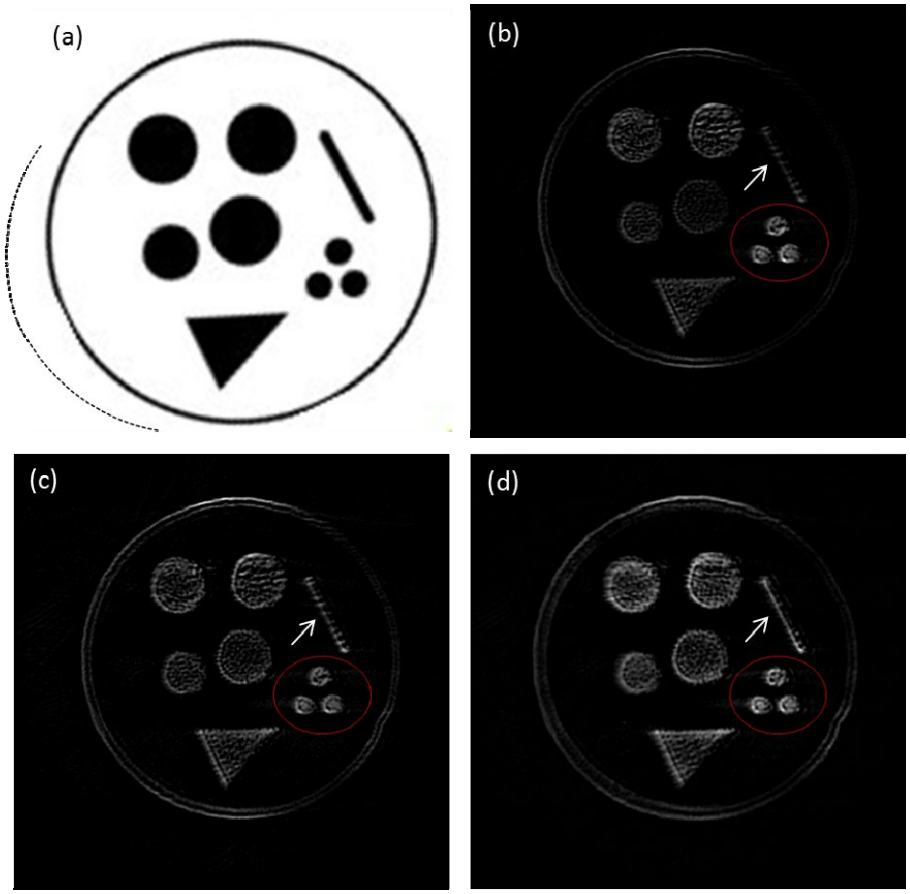

Figure 2. (a) the phantom structure, (b) the reference image without SR but using the same processing of SR reconstruction, (c) interleaving result, (d) SR result with 6 slices.

The results for the ex-vivo kidney experiment are presented in Fig. 3. A photograph of a cryoslice obtained through the imaging position is shown in Fig. 3(a). Fig.3(b) shows a reference image obtained with the FBP algorithm by considering 400x400 pixels with pixel width 50 μm. The interleaving result [Fig. 3(c)] obtained by directly registering information from different scanning views shows similar image fidelity to the reference image. In contrast, the PSR result considering 3 slices displayed in Fig. 3(d) demonstrates improvements on image quality. Specifically, blood vessel structures marked with the box indicated on Fig. 3(a) are better resolved in the PSR image than in the images obtained with other methods, as shown by inserts in Figs. 3(b-d). The vascular structures [as indicated by arrows in the inserts in Figs. 3(b-d)] in the PSR image show better structural integrity and conformity when compared to the LR image and the interleaving image. The visual evaluation is further corroborated by the line profile drawn over a given image segment [indicated by the yellow dash line in Fig. 3(b)], which confirms that the blood vessels are better illustrated in the PSR image.

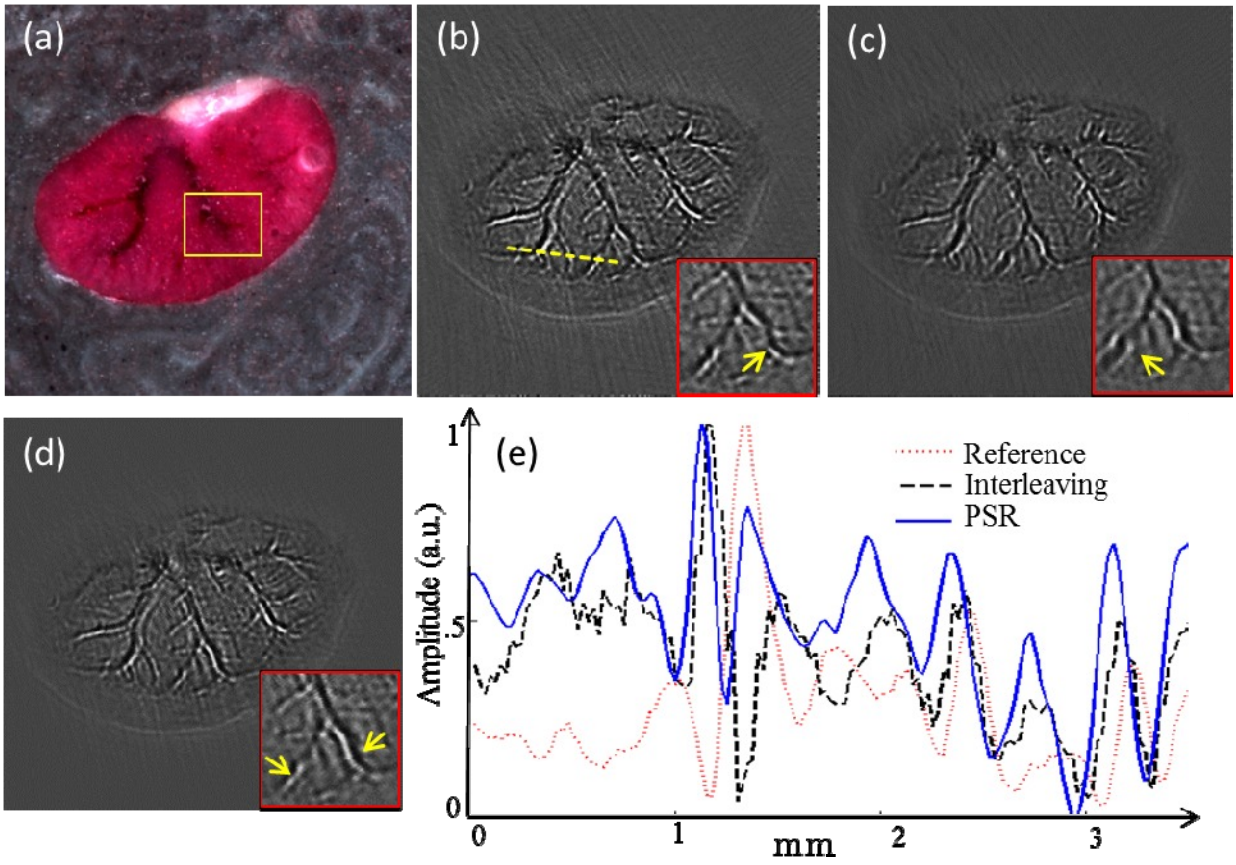

Figure .3. Imaging results for the ex-vivo murine kidney. (a) Reference cryoslice image. (b) Reconstructed high-resolution reference image. (c) Interleaving result with 3 images. (d) PSR image. The line profile as marked on (b) is shown in (e). Zoom in of the region marked in panel (a) is provided for better visualization of the image enhancement.

4. CONCLUSION

In this paper, the applicability of super-resolution image processing techniques for improving spatial resolution and image quality in optoacoustic tomographic imaging was demonstrated. The suggested super-resolution method makes use of multiple post-reconstruction optoacoustic images with geometrical overhead to efficiently integrate the information into a high-resolution image. The performance of the suggested method for enhancing image resolution and contrast was showcased for a specific cross-sectional imaging system. However, the method can easily be extended to a wide range of optoacoustic imaging systems by proper definition of the scanning protocol. In this way, simple geometrical manipulation can generally lead to an enhancement in optoacoustic contrast and resolution, thus overcoming limitations of the system hardware and reconstruction methods.

Funding. The research leading to these results has received funding from the European Union project FAMOS (FP7 ICT, contract no. 317744).

REFERENCES

[1] V. Ntziachristos, "Going deeper than microscopy: the optical imaging frontier in biology," *Nat Methods,* vol. 7, pp. 603-14, Aug 2010.

[2] P. Beard, "Biomedical photoacoustic imaging," *Interface Focus,* vol. 1, pp. 602-31, Aug 6 2011.

[3] A. Dima, N. C. Burton, and V. Ntziachristos, "Multispectral optoacoustic tomography at 64, 128, and 256 channels," *J Biomed Opt,* vol. 19, p. 36021, Mar 2014.
[4] S. Mandal, E. Nasonova, X. L. Dean-Ben, and D. Razansky, "Optimal self-calibration of tomographic reconstruction parameters in whole-body small animal optoacoustic imaging," *Photoacoustics,* vol. 2, pp. 128-136, Sep 2014.
[5] A. Buehler, X. L. Dean-Ben, D. Razansky, and V. Ntziachristos, "Volumetric optoacoustic imaging with multi-bandwidth deconvolution," *IEEE Trans Med Imaging,* vol. 33, pp. 814-21, Apr 2014.
[6] S. Farsiu, M. D. Robinson, M. Elad, and P. Milanfar, "Fast and robust multiframe super resolution," *IEEE Trans Image Process,* vol. 13, pp. 1327-44, Oct 2004.
[7] H. L. He, K. He, and G. Zou, "A Lorentzian Stochastic Estimation for Video Super Resolution with Lorentzian Gradient Constraint," *Ieee Transactions on Consumer Electronics,* vol. 58, pp. 1294-1300, Nov 2012.
[8] J. A. Kennedy, O. Israel, A. Frenkel, R. Bar-Shalom, and H. Azhari, "Super-resolution in PET imaging," *IEEE Trans Med Imaging,* vol. 25, pp. 137-47, Feb 2006.
[9] H. Greenspan, G. Oz, N. Kiryati, and S. Peled, "MRI inter-slice reconstruction using super-resolution," *Magnetic Resonance Imaging,* vol. 20, pp. 437-446, Jun 2002.
[10] G. Wang, M. W. Vannier, M. W. Skinner, M. G. Cavalcanti, and G. W. Harding, "Spiral CT image deblurring for cochlear implantation," *IEEE Trans Med Imaging,* vol. 17, pp. 251-62, Apr 1998.
[11] S. C. Park, M. K. Park, and M. G. Kang, "Super-resolution image reconstruction: A technical overview," *Ieee Signal Processing Magazine,* vol. 20, pp. 21-36, May 2003.
[12] B. E. Treeby, "Acoustic attenuation compensation in photoacoustic tomography using time-variant filtering," *J Biomed Opt,* vol. 18, p. 036008, Mar 2013.
[13] D. Razansky, A. Buehler, and V. Ntziachristos, "Volumetric real-time multispectral optoacoustic tomography of biomarkers," *Nat Protoc,* vol. 6, pp. 1121-9, Aug 2011.
[14] A. Buehler, E. Herzog, D. Razansky, and V. Ntziachristos, "Video rate optoacoustic tomography of mouse kidney perfusion," *Opt Lett,* vol. 35, pp. 2475-7, Jul 15 2010.